Fermion localization and resonances on two-field thick branes

C. A. S. Almeida,[1] R. Casana,[2] M. M. Ferreira, Jr.,[2] and A. R. Gomes[3]

[1]*Departamento de Física, Universidade Federal do Ceará (UFC), C. P. 6030, 60455-70, Fortaleza, Ceará, Brazil*
[2]*Departamento de Física, Universidade Federal do Maranhão (UFMA), Campus Universitário do Bacanga, 65085-580, São Luís, Maranhão, Brazil*
[3]*Departamento de Física, Instituto Federal de Educação, Ciência e Tecnologia do Maranhão (IFMA), 65025-001, São Luís, Maranhão, Brazil*

We consider (4, 1)-dimensional branes constructed with two scalar fields ϕ and χ coupled to a Dirac spinor field by means of a general Yukawa coupling. The equation of motion for the coefficients of the chiral decomposition of the spinor in curved spacetime leads to a Schrödinger-like equation whose solutions allow to obtain the masses of the fermionic modes. The simplest Yukawa coupling $\bar{\Psi}\phi\chi\Psi$ is considered for the Bloch brane model and fermion localization is studied. We found resonances for both chiralities and related their appearance to branes with internal structure.

I. INTRODUCTION

Braneworld scenarios have received great attention from the physical community after addressing important problems such as gauge hierarchy [1–3] and the cosmological constant [4,5]. The construction of domain walls embedded in a higher dimensional bulk, however, has a more ancient history in the literature [6–9]. As is well-known, (4, 1)-D branes can be classified as thin and thick ones. Thin branes are constructed after introducing a tension term in the action, localized by a Dirac delta function (see [10] and references therein). The mathematical formalism that describes the metric around the brane allows to obtain several interesting results in the domain of high energy physics and cosmology. Usually, the issue of field localization in such branes is addressed with the help of Dirac delta functions, without any clear subjacent dynamics. On the other hand, thick branes are constructed in a dynamical way after introducing one or more scalar fields coupled with gravity [11–14]. Thick branes are more natural in the sense that field and gravity localization can be studied with the introduction of smooth functions (instead of Dirac ones). Moreover, the thin brane solutions are recovered in certain limits [15,16]. One important issue in (4, 1)-D braneworld models is to consider spacetimes with a bulk metric that extends the Randall-Sundrum result [17] in a way that gravity can be localized in the (3, 1)-D slice [10,18–21]. The spacetime around the Randall-Sundrum brane is anti-de Sitter (AdS$_5$), and several thick brane models (that present this characteristic asymptotically) have been constructed.

Braneworld models with one or more scalar fields were constructed in order to relate gravity localization with brane thickness [22,23]. In particular, the Bloch brane model [23] is composed of two scalar fields and is the extension for the known Bloch walls [24–26] in the context of braneworlds. Bloch branes are stable structures that can be characterized as branes with interfaces located at the

maximum of energy density. The two interfaces signal the presence of an internal structure in the brane. The presence of an internal structure in topological defects was first considered in Witten's superconducting cosmic strings [27]. There the internal structure is provided by the condensation of a (charged) field over the defect. In the Bloch brane case, the appearance of internal structure is concerned with a low value of the coupling constant that guides the way the two fields interact with each other. For a stronger interaction, a single peak for the energy density characterizes a brane with simpler structure. It was also shown [23] that in the presence of gravity the interfaces are located more closely in the extra dimension. As such branes are able to localize gravity, one interesting question is investigating how fermionic fields may be localized. In this way, there arises the expectation that a brane with richer internal structure could provide new results when compared to a simple kinky brane.

The study of fermion localization on branes [28–40] is rich and interesting. In order to localize fermions in branes one needs a coupling between the spinors and the scalar fields that form the brane. This is a condition also present in Jackiw and Rebbi treatment of fermion localization on solitons in flat space [41]. In branes, the procedure consists in separating from the full spinor one scalar coefficient with dependence only on the extra dimension, leading to a Schrödinger-like equation and a probabilistic interpretation. Depending on the model, one can obtain resonant massive states.

In particular, the authors of [37] analyzed the issue of fermion localization on a brane constructed with the sine-Gordon potential. That work considered general fermionic Yukawa couplings between one scalar field and spinorial fields. It was found that the simplest Yukawa coupling $\bar{\Psi}\phi\Psi$ allowed left-handed fermions to possess a zero mode that localizes on the brane. The right-handed fermions, on the other hand, present no zero mode. The large

massive fermionic modes (for both left and right chirality) are plane waves and thereby are not localized on the brane.

Inspired on the results obtained in [37], we investigate the issue of fermion localization of fermions on a brane constructed from two scalar fields coupled with gravity. In Sec. II, we present the known first-order equations for a brane model coupled with scalar fields [11]. Sec. III deals with the fermionic sector of the model, where we extend the results from [37] for two scalar fields ϕ and χ with general coupling. Afterwards, we choose the simple coupling $\bar{\Psi}\phi\chi\Psi$. In Sec. IV, we consider the Bloch brane model and our main results are presented. The Schrödinger-like equation for the model is obtained and numerically solved. The solutions correspond to massive fermionic modes. We have found resonances on the brane and have related their appearance with the simultaneous increasing of the brane internal structure. Our conclusions are presented in Sec. V.

II. SCALAR FIELD AND METRIC EQUATIONS

Our system is described by the action

$$
S = \int d^4x dy \sqrt{|g|} \left[-\frac{1}{4}R + \frac{1}{2}\partial_a\phi\partial^a\phi + \frac{1}{2}\partial_a\chi\partial^a\chi - V(\phi,\chi) \right],
\tag{1}
$$

and the metric

$$
ds^2 = g_{ab}dx^a dx^b, \qquad ds^2 = e^{2A}\eta_{\mu\nu}dx^\mu dx^\nu - dy^2,
\tag{2}
$$

where $g = \det(g_{ab})$. Here $a, b = 0, 1, 2, 3, 4$, and e^{2A} is the warp factor. We suppose that $A = A(y)$, $\phi = \phi(y)$ and $\chi = \chi(y)$. The extra dimension y is infinite, and we have the continuity of the first derivatives of $\phi(y)$, $\chi(y)$ and $A(y)$ with respect to y as boundary conditions for the thick brane.

The action given by Eq. (1) leads to the following coupled differential equations for the scalar fields $\phi(y)$, $\chi(y)$ and the function $A(y)$ from the warp factor:

$$
\phi'' + 4A'\phi' = \frac{\partial V(\phi,\chi)}{\partial\phi},
\tag{3}
$$

$$
\chi'' + 4A'\chi' = \frac{\partial V(\phi,\chi)}{\partial\chi},
\tag{4}
$$

$$
A'' = -\frac{2}{3}(\phi'^2 + \chi'^2),
\tag{5}
$$

$$
A'^2 = \frac{1}{6}(\phi'^2 + \chi'^2) - \frac{1}{3}V(\phi,\chi),
\tag{6}
$$

where prime stands for derivative with respect to y.

With the potential [11],

$$
V(\phi,\chi) = \frac{1}{8}\left[\left(\frac{\partial W}{\partial\phi}\right)^2 + \left(\frac{\partial W}{\partial\chi}\right)^2\right] - \frac{1}{3}W^2,
\tag{7}
$$

the first-order differential equations which also solve the equations of motion are

$$
\phi' = \frac{1}{2}\frac{\partial W}{\partial\phi},
\tag{8}
$$

$$
\chi' = \frac{1}{2}\frac{\partial W}{\partial\chi},
\tag{9}
$$

$$
A' = -\frac{1}{3}W.
\tag{10}
$$

III. FERMIONIC SECTOR

Now, we consider a Dirac spinor field coupled with the scalar fields by a general Yukawa coupling. The action for this sector is

$$
S = \int d^5x\sqrt{-g}[\bar{\Psi}\Gamma^M D_M\Psi - \eta\bar{\Psi}F(\phi,\chi)\Psi].
\tag{11}
$$

Here we consider the fields ϕ and χ as background fields given as solutions of the Eqs. (3)–(6). In other words, we neglect the backreaction from the spinor field on the brane solutions.

We change variable from y to z with

$$
z = \int_0^y e^{-A(\xi)}d\xi,
\tag{12}
$$

in order to rewrite Eq. (2) and get a conformally flat metric

$$
ds^2 = e^{2A}(\eta_{\mu\nu}dx^\mu dx^\nu - dz^2).
\tag{13}
$$

This change of variable is usual in problems of gravity localization. Indeed, for a large class of models, one can achieve a Schrödinger-like form for the equations for metric fluctuations, when decoupled from the scalar fluctuations in a specific gauge. In the treatment of fermion localization the same change of variable is used. The equation of motion corresponding to the action given by Eq. (11) is

$$
[\gamma^\mu\partial_\mu + \gamma^5(\partial_z + 2\partial_z A) - \eta e^A F(\phi,\chi)]\Psi = 0.
\tag{14}
$$

We apply the well-known procedure of a general chiral decomposition for the spinor Ψ:

$$
\Psi(x,z) = \sum_n \psi_{Ln}(x)\alpha_{Ln}(z) + \sum_n \psi_{Rn}(x)\alpha_{Rn}(z),
\tag{15}
$$

where the sum can be over discrete bounded modes or over a continuum of modes. In this decomposition $\psi_{Ln}(x)$ and $\psi_{Rn}(x)$ are, respectively, the left-handed and right-handed components of the four-dimensional spinor field with mass m_n. Also, there are two scalars α_{Ln} and α_{Rn} that depend

only on the extra dimension z. In order to turn the notation easier, we dropped the index n in which follows. After applying Eq. (15) in Eq. (14), we obtain two equations for the scalars α_L and α_R:

$$[\partial_z + 2\partial_z A + \eta e^A F(\phi, \chi)]\alpha_L(z) = m\alpha_R(z), \qquad (16)$$

$$[\partial_z + 2\partial_z A - \eta e^A F(\phi, \chi)]\alpha_R(z) = -m\alpha_L(z). \qquad (17)$$

Implementing the change of variables $\alpha_L = e^{-2A}L$ and $\alpha_R = e^{-2A}R$ [37], we get Schrödinger-like equations for the wave functions $R_m(z)$ and $L_m(z)$ given by

$$H_L L_m(z) = m^2 L_m(z), \qquad (18)$$

$$H_R R_m(z) = m^2 R_m(z), \qquad (19)$$

with corresponding Hamiltonians

$$H_L = \left(-\frac{d}{dz} + e^A \eta F\right)\left(\frac{d}{dz} + e^A \eta F\right), \qquad (20)$$

$$H_R = \left(\frac{d}{dz} + e^A \eta F\right)\left(-\frac{d}{dz} + e^A \eta F\right). \qquad (21)$$

The structure of the Hamiltonians guarantees that m is real, the absence of tachyonic modes and the possibility of interpreting $|R_m(z)|^2$ and $|L_m(z)|^2$ as the probability for finding the right and left massive modes in a given coordinate z. The Schrödinger equations can be also written explicitly as

$$-L_m''(z) + V_L(z)L_m(z) = m^2 L_m, \qquad (22)$$

$$-R_m''(z) + V_R(z)R_m(z) = m^2 R_m, \qquad (23)$$

with

$$V_L(z) = e^{2A}\eta^2 F(\phi, \chi)^2 - e^A \eta \partial_z F(\phi, \chi) - (\partial_z A)e^A \eta F(\phi, \chi), \qquad (24)$$

$$V_R(z) = e^{2A}\eta^2 F(\phi, \chi)^2 + e^A \eta \partial_z F(\phi, \chi) + (\partial_z A)e^A \eta F(\phi, \chi), \qquad (25)$$

named as the Schrödinger-like potentials for the fermionic fields. The Hamiltonians from Eqs. (20) and (21) can be written as $H_L = A^\dagger A$ and $H_R = AA^\dagger$. This shows that H_L and H_R are conjugated Hamiltonian of supersymmetric quantum mechanics and $V_L(z)$ and $V_R(z)$ are superpartner potentials. In this way there is a zero mode for $V_L(z)$ and the spectra of $V_L(z)$ and $V_R(z)$ are interrelated [42,43].

From now on, we consider the simplest Yukawa coupling $F(\phi, \chi) = \phi\chi$ and study the occurrence of massive modes for the known Bloch brane model with two scalar fields.

IV. THE BLOCH BRANE MODEL

A rich model that leads to branes with internal structure is [24–26]

$$W(\phi, \chi) = 2\phi - \frac{2}{3}\phi^3 - 2a\phi\chi^2, \qquad (26)$$

with a being a real parameter $(0 < a < 0.5)$. In this case, the first-order Eqs. (8)–(10) can be solved analytically, leading to the following results [23]:

$$\phi(y) = \tanh(2ay), \qquad (27)$$

$$\chi(y) = \sqrt{\left(\frac{1}{a} - 2\right)}\text{sech}(2ay), \qquad (28)$$

and

$$A(y) = \frac{1}{9a}[(1 - 3a)\tanh^2(2ay) - 2\ln\cosh(2ay)]. \qquad (29)$$

Figure 1(a) shows how the warp factor tends to zero going to the AdS$_5$ limit far from the brane. The brane thickness decreases with a, and this can be seen by the plots of the field solutions in Figs. 1(b) and 2(a).

Now, we turn to the z-variable according to Eq. (12). For general values of a, the expression for $A(y)$ from Eq. (29) is not suitable to be integrated in a known explicit form and numerical methods are necessary. However, for the particular case $a = 1/3$ we have

$$A(y) = -\frac{2}{3}\ln\cosh(2ay), \qquad (30)$$

and

$$z = \int_0^y \left[\cosh\left(\frac{2}{3}y\right)\right]^{2/3}. \qquad (31)$$

After simple integration, we get an expression for $z(y)$ in an explicit form in terms of an hypergeometric function:

$$z = \frac{y}{|y|}\left[\frac{9}{4}\left(\cosh\left(\frac{2}{3}y\right)\right)^{2/3}{}_2F_1\left(-\frac{1}{3}, \frac{1}{2}; \frac{2}{3}; \left(\cosh\left(\frac{2}{3}y\right)\right)^{-2}\right) - \frac{9}{8\pi}\Gamma\left(\frac{2}{3}\right)\Gamma\left(\frac{5}{6}\right)\right]. \qquad (32)$$

Unfortunately, even in this simpler case, we can not obtain the inverse $y(z)$ in an explicit form. However, this explicit form for $z(y)$ is already useful to produce sequences of pairs of points (z, y) with a constant step in z. Indeed, given a value z, the corresponding y can be found after numerically solving the implicit equation [Eq. (32)]. This leads to the determination of the functions $\phi(z)$, $\chi(z)$, $A(z)$ with good precision. The corresponding derivative with respect to z, $A'(z)$, can be found as

$$\frac{dA}{dz} = \frac{dA}{dy}\frac{dy}{dz} = \frac{dA}{dy}\left(\cosh\frac{2}{3}y\right)^{-2/3}, \qquad (33)$$

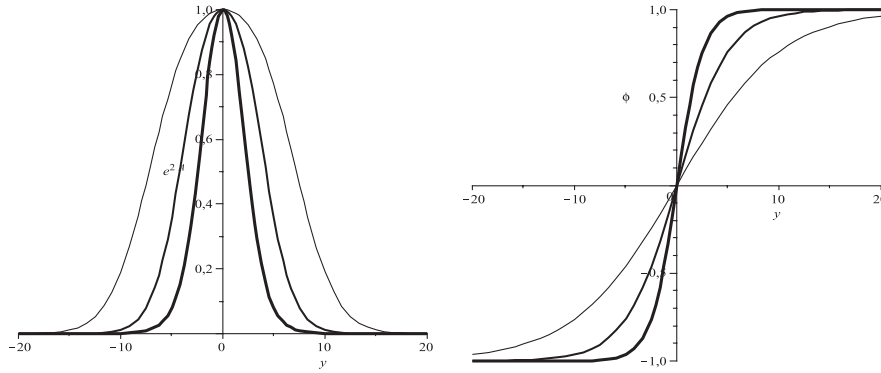with dA/dy stemming from the explicit expression for $A(y)$

FIG. 1.   (a) Warp factor $e^{2A(y)}$ (left) and (b) field $\phi(y)$ (right) for $a = 0.05$ (thinner trace, larger curves), $a = 0.10$ and $a = 0.20$ (thicker trace, narrower curves).
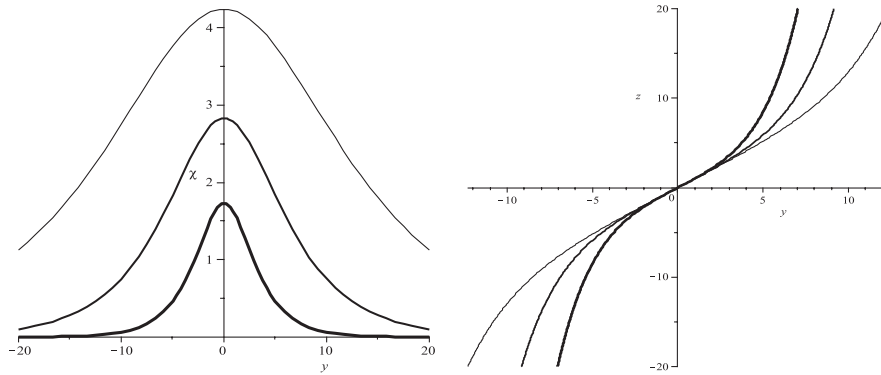

FIG. 2.   (a) Field $\chi(y)$ (left) and (b) function $z(y)$ (right) for $a = 0.05$ (thinner trace, larger curves), $a = 0.10$ and $a = 0.20$ (thicker trace, narrower curves).

(Eq. (30)). Similarly, we can construct the functions $\phi'(z)$, $\chi'(z)$. All the former calculations can be used to construct the Schrödinger potentials V_L and V_R displayed in Fig. 3 with good precision; this was used with the purpose of validating the numerical method used for general values of a.

For some values of a, we integrated numerically Eq. (12) obtaining $z(y)$, whose graphic is depicted in Fig. 2(b). With

this, we can numerically determine $A(z)$, $\phi(z)$, $\chi(z)$. In order to obtain the derivatives $A'(z)$, $\phi'(z)$, $\chi'(z)$, a numerical procedure was constructed for generating sequences with constant step in z. In this way the procedure for general values of a is more involved once we do not have an explicit form for $z(y)$ to guide us as in the $a = 1/3$ previous case. Equations (24) and (25) are then used to provide a graphical form for the potentials V_L and V_R. We
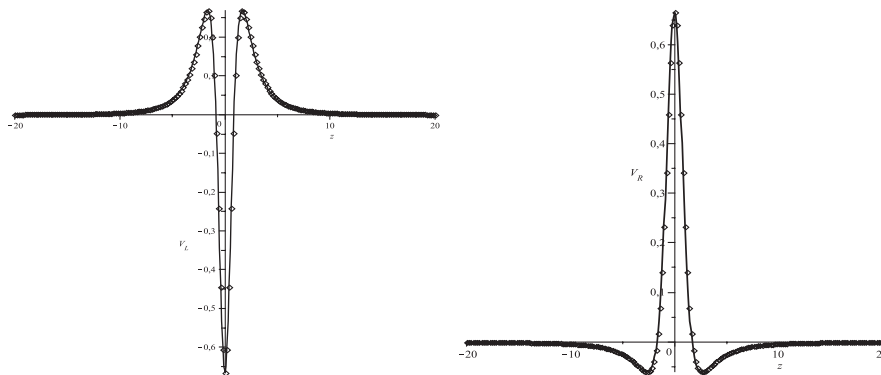

FIG. 3.   Comparing procedures: Schrödinger-like potential (b) $V_L(z)$ (left) and (c) $V_R(z)$ (right) for $a = 1/3$, obtained with explicit function $z(y)$ (points) and with the full numerical procedure (line). Note that both procedures give almost indistinguishable results.
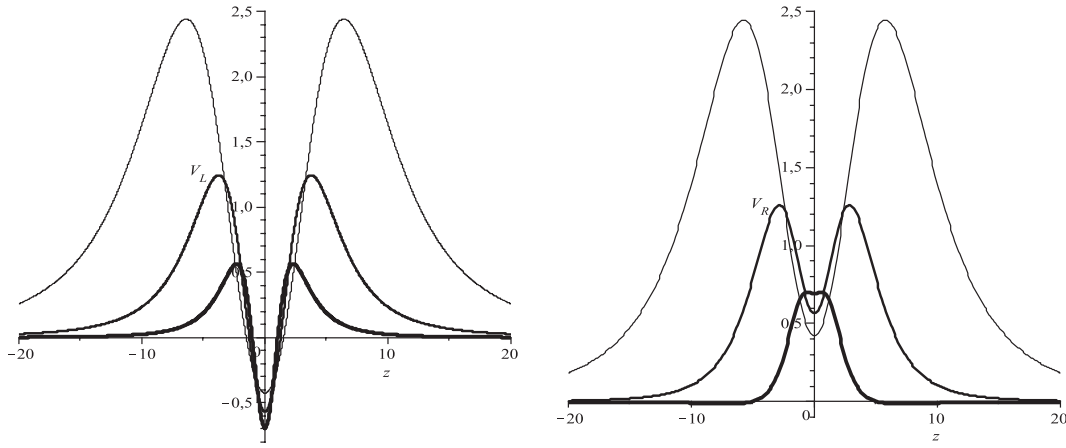
FIG. 4.   Schrödinger-like potentials (a) $V_L(z)$ (left) and (b) $V_R(z)$ (right) for $a = 0.05$ (thinner trace), $a = 0.10$ and $a = 0.20$ (thicker trace).

applied this procedure for the $a = 1/3$ case, whose results are depicted in Figs. 3(a) and 3(b). Such graphics reveal that both procedures described here lead to almost the same results.

Now, we can use the general numerical procedure to investigate the potential V_L for other values of a. Some results are exhibited in Fig. 4(a). We note from this figure that V_L has a volcanolike shape, that goes asymptotically to zero far from the brane. This form of potential is usually found in problems involving gravity localization. Here, we can search for the existence of a zero mode followed by a continuum of massive modes by means of an analogy. Indeed, we note that the potential is negative at the brane location; this guarantees the existence of a normalized zero mode after integrating Eq. (18) for $m = 0$:

$$L_0 \propto \exp\left(-\eta \int_0^z dz' e^{A(z')} \phi(z')\chi(z')\right). \quad (34)$$

Figure 4(b) shows that the potential V_R is always positive at the brane position, which is not compatible with the existence of bound fermions with right chirality. However, we note the appearance of a hole in the potential that grows for lower values of a. This fact is new and our hypothesis is that it can be related, in some way, to the internal structure [22] of the brane constructed with two fields. It is remarkable that such behavior of the V_R potential was not observed in a previous treatment for one-field models. The appearance of this hole in the potential can be responsible for resonances or at least for a light increase in the decay rate of massive fermions on the brane. Note also that the hole around $z = 0$ for V_R is absent for larger values of a, in principle prohibiting the existence of resonances for this range of parameter. In order to look for resonant effects, we must consider now the massive modes, solving numerically the Schrödinger-like equation with purely numeric potentials.

A. Right-handed fermions

Firstly we will consider the case of right-handed fermions with the small parameter $a = 0.05$. We can vary m^2 to get the wave functions $R_m(z)$. Equation (23) shows that we need two initial conditions. As we are dealing with thick brane with no tension at $z = 0$, the Israel junction conditions applied to the brane give $R(z)$ and $R'(z)$ continuous at $z = 0$. Note that the absence of negative values for the potential V_R prohibits the existence of bound states. However, the tunneling process across the barrier (localized at the region between the maximum of the potential and the origin) can result in different rates for the leaking process depending on the mass of the modes. Here the region of interest corresponds to masses satisfying $0.42 < m^2 < 2.44$, where the tunneling process is effective (see Figure 4(b)—thinner trace).

Figures 5(a)–5(d) shows typical even massive fermionic modes before normalization for the region $z > 0$. Figures 5(a)–5(c) belongs to the more interesting region $0.42 < m^2 < 2.44$ whereas Fig. 5(d) is for a higher massive mode. The lower massive modes show that there is a transient behavior followed by typical plane wave oscillations, characteristic of a free mode. This shows that these modes represent massive fermions that certainly will be leaked from the brane. Comparing Fig. 5(a) with Figs. 5(b) and 5(c), we note that the transition region roughly corresponds to $-20 < z < 20$. Note also that for lower values of m^2 the values of the non-normalized wave functions $R(z)$ depart largely from the initial value 1. More important is to estimate how larger is the solution $R(z)$ in the transition region $-20 < z < 20$ in comparison to the amplitude of the plane wave oscillations. Indeed, one would expect that broader differences would correspond to greater lifetimes for the massive fermionic states near to the brane. This difference assumes a huge amount for $m^2 = 2.1$, as we can see from Fig. 5(c).

This lead us to the point of normalization of the massive modes and to the better estimate of $R_m(0)$. Their impor-
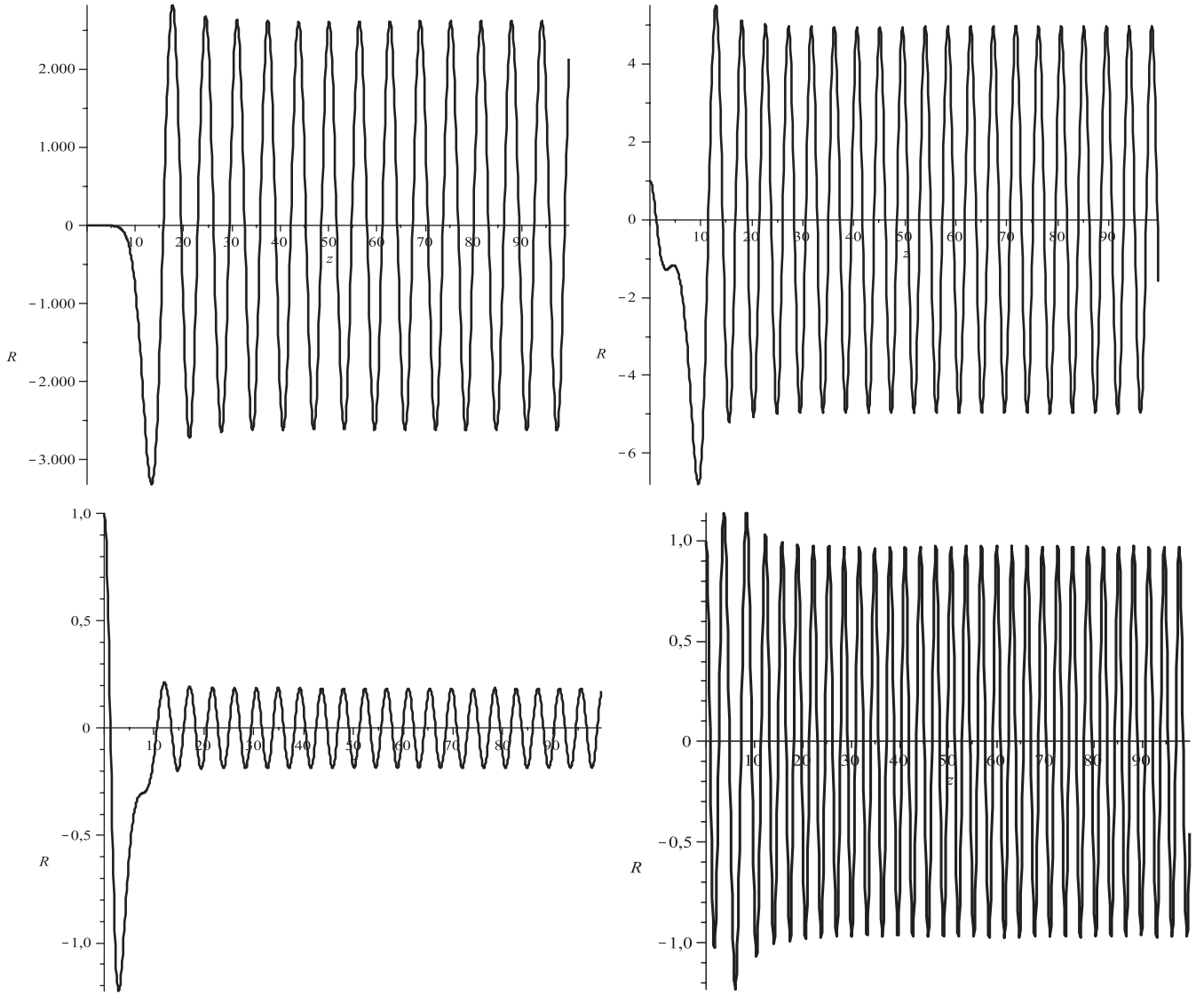
FIG. 5. Non-normalized even massive right-handed fermionic modes for $a = 0.05$ with (a) $m^2 = 1$ (upper left), (b) $m^2 = 2$ (upper right), (c) $m^2 = 2.1$ (lower left) and (d) $m^2 = 4$ (lower right).

tance is that we can rewrite Eq. (23) as $\mathcal{O}_R^\dagger \mathcal{O}_R R(z) = m^2 R(z)$, which ensures that we can interpret $|R_m(0)|^2$ as the probability for finding the massive modes on the brane. In particular, large peaks in the distribution of $R(0)$ as a function of m would reveal the existence of resonant states closely related to the existence of a brane with internal structure.

We can consider a normalization procedure for the wave functions $R_m(z)$ in a box with borders located far from the turning point, where the solutions have characteristics of plane waves toward the brane. In this way, we considered a box with $-100 < z < 100$. An important information can be obtained from the normalized $|R_m(0)|^2$, since from it we can compare the relative probability for finding a massive mode on the brane. The result is depicted in Fig. 6(a). We note from the figure a huge peak around $m^2 = 2.1$, char-

acterizing the occurrence of a resonance and a long-lived massive fermionic mode on the brane. We note from the figure that low massive modes have negligible associated probabilities, whereas high massive modes are character-ized by a plateau in the probability distribution. This is related to the finite size of the box used for normalization. Indeed, for $m^2 \gg V_R$ we can approximate the Schrödinger equation as $-R''(z) \sim m^2 R(z)$, with normalized solution $R(z) \sim 1/\sqrt{z_{\max}} \cos(mz)$, where $2z_{\max}$ is the size of the box used for normalization. For our choice $z_{\max} = 100$, we have $|R(0)|^2 = 1/(z_{\max}) = 0.01$, corresponding to the pla-teau observed in Fig. 6(a).

Since in our model the extra dimension is infinite, one may wonder about the influence of $z_{\max}$ on the normaliza-tion of the spectral density. Indeed, another choice of $z_{\max}$ would lead to another plateau in the probability distribu-
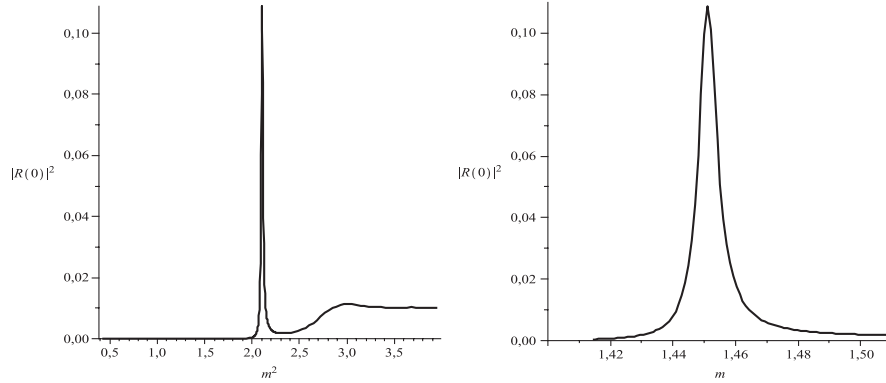
FIG. 6.   (a) Normalized squared wave function for a right-handed fermion on the brane, $|R(0)|^2$, as a function of m^2. Note the high peak characteristic of resonance. For the present case we have $a = 0.05$. (b) Normalized squared wave function for a right-handed fermion on the brane, $|R(0)|^2$, as a function of m, identifying better the region defining the peak of resonance.

tion. The physical information, however, is contained in the value of the resonance peak, which does not depends on z_{max} since it is chosen sufficiently large.

Figure 6 shows the peak of resonance with the horizontal scale now taken as m. We can estimate the lifetime τ for the observed resonance from the width at half maximum of the peak appearing in the figure. Indeed, the width in mass $\Gamma = \Delta m$ of the peak is related to the lifetime. In this way, in its own reference frame, the fermion disappears toward the extra dimension with time scale $\tau \sim \Gamma^{-1}$ [44]. The peak was located at $m = 1.451(1)$ with the maximum probability around 0.109. The width at half maximum is $\Delta m = 0.0083$, resulting in a lifetime $\tau_a = \tau_{0.05} = 120$. These results are in arbitrary units, and their significance will be better understood after comparison with the results for other values of the parameter a.

Now, we repeat our analysis for other values of a to investigate the effects of the coupling parameter a between the fields ϕ and χ for the existence of resonances and their lifetimes.

For $a = 0.10$ the results for $|R(0)|^2$, as a function of m^2, are depicted in Fig. 7(a). Note from the figure that we also

have one resonant peak as before. Now, however, the larger value of a results in a smaller value of the mass for the resonant state. Also, the resonant peak is more pronounced. Figure 7(b) shows that the peak was located at $m = 0.968$ with the maximum probability around 0.202. The width at half maximum is $\Delta m = 0.02$, resulting in a lifetime $\tau_a = \tau_{0.1} = 50$. Comparing this result with $\tau_a = \tau_{0.05} = 120$, we conclude that smaller values of a result in resonances with larger lifetimes.

We compare both cases in Fig. 8, where we display the resonances for $a = 0.05$ (second smaller peak) and $a = 0.10$ (first larger peak). We know that smaller values of a correspond to branes with a richer internal structure [23]. Then the observed thinner peaks for smaller parameters a mean resonances more pronounced and a trapping mechanism more effective. This is connected with the larger amount of matter now forming the brane due to the coupling of the scalar field ϕ to the other field χ.

The reduction of the lifetime for resonances with larger values of a poses the question if there are no resonances at all on the brane for values of a above a certain threshold a^*. We noted the decreasing of the associated mass for the
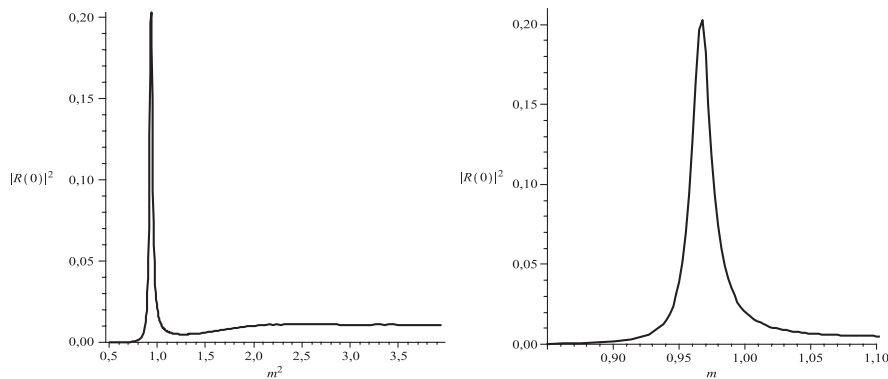

FIG. 7.   (a) Normalized squared wave function for a right-handed fermion on the brane, $|R(0)|^2$, as a function of m^2, for $a = 0.10$ and $-100 < z < 100$. (b) Normalized squared wave function for a right-handed fermion on the brane, $|R(0)|^2$, as a function of m, identifying better the region defining the peak of resonance.
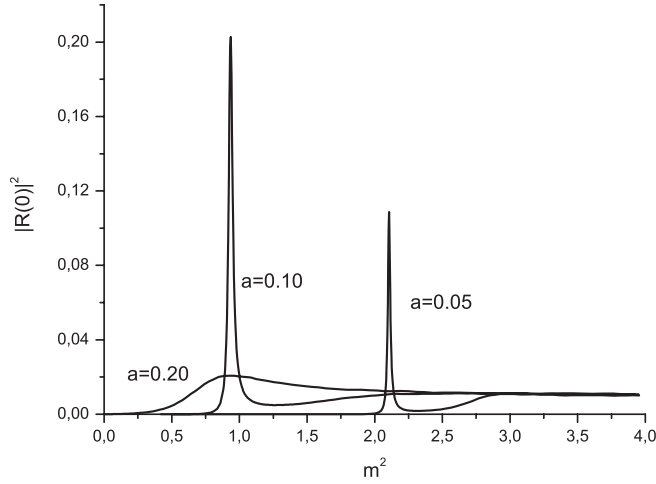
in Ref. [23]. The energy density $T_{00}^a(y)$ as a function of the coordinate y and for a fixed parameter a is given by

$$T_{00}^a(y) = e^{2A(r)}\left[\frac{1}{2}\left[\left(\frac{d\phi(y)}{dy}\right)^2 + \left(\frac{d\chi(y)}{dy}\right)^2\right]\right.$$

$$\left. + V(\phi(y), \chi(y))\right]. \qquad (35)$$

Figure 10 shows that the structure of the brane changes when the parameter is $a = 0.17$. Indeed, we note that for $0.17 < a < 0.5$ the energy density characterizes a defect with the energy density centered around a central peak, whereas for $a < 0.17$ the appearance of two symmetric peaks signals the occurrence of a brane with internal structure (more details in Ref. [23]). Now, we connect this known result with our findings of resonance peaks for small values of a and with the absence of such resonances for larger values of a. There appears to be a connection between the occurrence of metastable states on the brane and the occurrence of two peaks in the energy density characterizing these branes. From this we conclude that branes with internal structure favor the appearance of resonance states for right-handed fermions. Also, for branes without internal structure, we were not able to find resonance states.

A further point to remark is that we have considered analytical fittings for the Schrödinger potentials $V_R(z)$ in terms of finite series with oscillating terms. For fittings that agreed visually with our numerical points, the Runge-Kutta method was applied and the normalized massive modes were constructed. The results for the resonances were roughly the same, corroborating our conclusions.

B. Left-handed fermions

For left-handed fermions, as we already noted, there is a normalized zero mode. We repeated the analysis from the previous section and also found resonances. However, for left-handed fermions there are differences with respect to the position of the resonance peak, in comparison to which
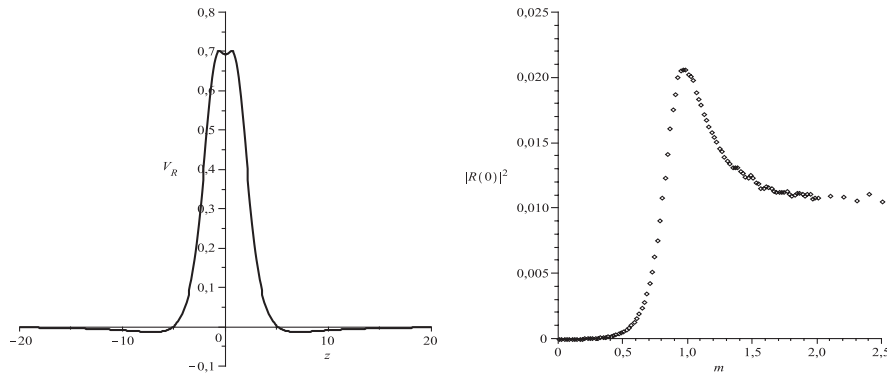

FIG. 8.   Normalized squared wave function for a right-handed fermion on the brane, $|R(0)|^2$, as a function of m^2. We used $-100 < z < 100$, and the resonant peaks correspond to $a = 0.05$ (third narrow and smaller peak), $a = 0.10$ (higher peak). Also it is showed the broader peak for $a = 0.20$.

resonances with larger values of a. Also, it was noted a qualitative change on the potential V_R above a certain value a^*. For example, for $a = 0.20$, Fig. 9(a) shows that now the potential assumes the form of a volcano. One characteristic of this type of potential is the occurrence of a zero mode when the central part, around the brane, assumes negative values. This is the potential observed in Fig. 4(a) for left fermions. Here, however, the central part of the potential is positive and the zero mode is absent. For $a = 0.20$ there were observed no resonances on the brane. In fact, Fig. 9(b) depicts the probability $|R(0)|^2$ as a function of the mass of excitations. Here we can see that the width at half maximum Δm is larger that the position of the peak $m = 0.95(1)$. This characterizes a state with a lifetime $\tau = 1/\Delta m$ too small to result in any physical effect, characterizing the absence of a resonant state.

We can relate these results with the behavior of the energy density of the brane without fermions as studied

FIG. 9.   (a) Schrödinger-like potential $V_R(z)$ for $a = 0.20$. Note the appearance of a region with negative potential, absent for the lower values of a considered previously. (b) Normalized squared wave function a for right-handed fermion on the brane, $|R(0)|^2$, as a function of m. Note now the presence of a broader peak with $\Delta m > m$.
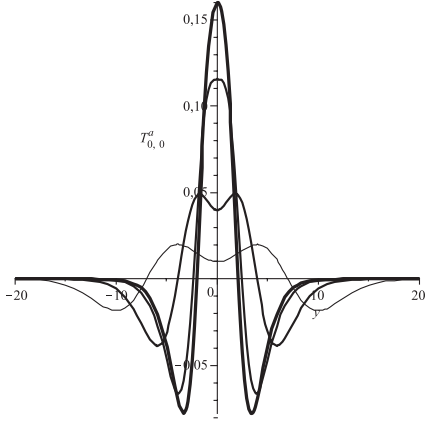
FIG. 10.   (a) Plots of the matter energy density $T_{00}^{0.05}(y)$ (thinner trace), $T_{00}^{0.10}(y)$, $T_{00}^{0.17}(y)$ and $T_{00}^{0.20}(y)$ (thicker trace).

was obtained for right-handed ones. For instance, for $a = 0.05$, we found a resonance peak around $m = 1.59$, with $\Delta m = 0.07$, corresponding to a lifetime $\tau = 14$. When comparing with corresponding results for right-handed fermions ($m = 1.45$ and $\tau = 120$), we see that the left-handed resonance is the more massive and the less stable. Analysis for the resonance peak for $a = 0.10$ showed that, similarly to the observed for right-handed fermions, an increasing a also thickens the resonance peak for left-handed fermions.

C. Correspondence between the spectra and realization of Dirac fermions

The lack of correspondence between the spectra of left- and right-handed fermions appears to be in contradiction to the fact that V_L and V_R are superpartner potentials. The reason for this is that the parity-odd modes do not couple to the four-dimensional braneworld at $z = 0$, because for such modes we have $R(0) = 0$ and $L(0) = 0$. This was also noted in the case of gravity localization in another

model [45]. After we submitted this work, we knowed about Ref. [46], where a study of odd parity modes is done. According to ref. [46], we set $L(0) = 0$ and $L'(0) = 5$ for parity-odd wave functions as our starting point for the application of the numerical Numerov method. We use the scheme with step h in z corresponding to the points z_i described by

$$L(0) = 0, \tag{36}$$

$$L(h) = hL'(0), \tag{37}$$

$$L(z_i) = \frac{2[1 + 5F(z_{i-1})]L(z_{i-1}) - [1 - F(z_{i-2})]L(z_{i-2})}{1 - F(z_i)}, \tag{38}$$

where

$$F(z) = -\frac{1}{12}h^2(V_L(z) - m^2). \tag{39}$$

The condition $L'(0) = 5$ is arbitrary and will be fixed after the normalization process.

Thick branes are extended objects along the extra dimension that allow us to interpret, after normalizing $L(z)$, the probability for finding the massive modes on the brane (not necessarily at $z = 0$) as $\int_{-z_b}^{z_b} dz |L_m(z)|^2$. The parameter z_b is chosen in order to allow the influence of the odd modes in small regions around $z = 0$. We can consider a normalization procedure for the wave functions $L_m(z)$ in a box with borders located at $z = \pm z_{max}$, far from the turning point, where the solutions have characteristics of plane waves far from the brane. After normalization of $L(z)$, the probability for finding the massive modes on the brane is given by [46]

$$P_{brane} = \frac{\int_{-z_b}^{z_b} dz |L_m(z)|^2}{\int_{-z_{max}}^{z_{max}} dz |L_m(z)|^2}. \tag{40}$$

We followed the same procedure for right-handed fermions
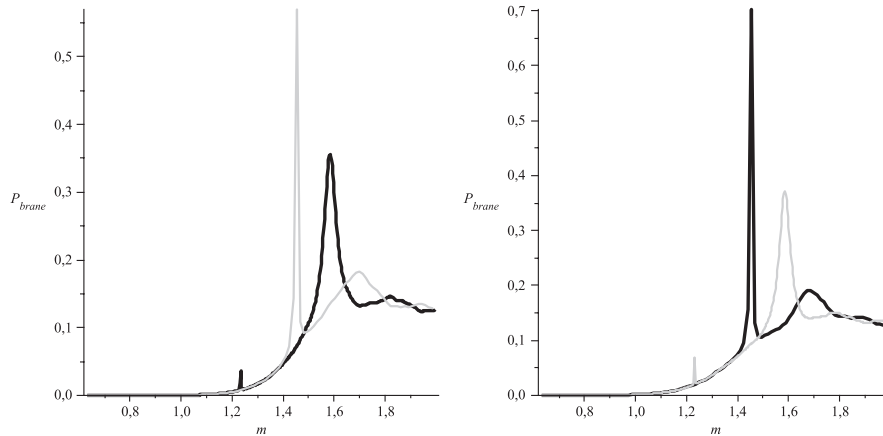

FIG. 11.   Plots of P_{brane} for $z_{max} = 100$, $z_b = 10$, $a = 0.05$. Curves for a) V_R (left) and b) V_L (right) constructed with even (thicker trace) and odd (thinner gray trace) wave functions.

and depicted in Fig. 11 the results for P_{brane} in the particular case of $a = 0.05$. The values of m for the resonance peaks in the figure corresponding to the parity even wave functions agree with the obtained previously in the plots of the normalized $|R(0)|^2$ [Fig. 6(b)] and $|L(0)|^2$. The figure also shows that with this procedure the resonance peaks for left- and right-quirality agree with good precision and the formation of Dirac fermions is realized. Larger values of the parameter z_b do not change the results for the position of the resonance peaks, but small values of z_b are more efficient to identify the peaks. One example of such procedure in a model with three thin branes was done in Ref. [30], where one of the wave functions (right or left-handed) is symmetric and the other corresponding to the same mass is antisymmetric with respect to the center of the orbifold. This is a consequence of demanding the action to be even under the Z_2 orbifold symmetry [47]. In this way it is shown the existence of metastable massive Dirac modes trapped on the brane. In our case of one thick brane immersed in a bulk with infinite extra dimension, if we allow measurements only at $z = 0$, the evidence of Dirac fermions is lost. In the more realistic scenario, one must consider the finite size of the brane and a nonzero overlap between the parity-odd wave functions with the SM fields [47], which would be sensitive to the extra dimension in the vicinity of the brane, justifying the procedure followed in this section.

D. Dimensional analysis and phenomenology

After restoring the dimensional parameters in the action (1), it reads as

$$S = \int dx^4 dy \sqrt{|g|} \left[-\frac{1}{4G^{(5)}} R + \frac{1}{2} g^{ab} \partial_a \phi \partial_b \phi \right.$$
$$\left. + \frac{1}{2} g^{ab} \partial_a \chi \partial_b \chi - V(\phi, \chi) \right]. \quad (41)$$

In a five-dimensional spacetime, the mass dimension for the fields and coupling constants in the action are: $[\phi] = [\chi] = M^{3/2}$, $[V(\phi, \chi)] = M^5$, $[g_{ab}] = 1$, $[R] = M^2$ and the five-dimensional gravitational constant has dimension $[G^{(5)}] = M^{-3}$.

The potential of the scalar fields (7) is written as

$$V(\phi, \chi) = \frac{1}{8} \left(\frac{\partial W}{\partial \phi} \right)^2 + \frac{1}{8} \left(\frac{\partial W}{\partial \chi} \right)^2 - \frac{1}{3} G^{(5)} W^2, \quad (42)$$

where W is the superpotential with mass dimension 4. The coupling $G^{(5)}$ in the last term guarantees the possibility of the model to have some compatibility with the expected LHC phenomenology.

In that way, the Bloch brane is defined by the following superpotential

$$W = 2\kappa Z \phi - \frac{2\kappa}{3Z} \phi^3 - \frac{2a\kappa}{Z} \phi \chi^2 \quad (43)$$

with $[Z] = M^{3/2}$, $[\kappa] = M$ and $[a] = 1$. It yields the following solutions for the scalar fields

$$\phi = Z \tanh(2a\kappa y), \qquad \chi = Z \left(\frac{1}{a} - 2 \right)^{1/2} \cosh^{-1}(2a\kappa y), \quad (44)$$

where Z, the kink amplitude, is given in terms of the five-dimensional gravitational constant as $Z^{-2} = G^{(5)}$ and, the parameter κ^{-1} is related with the brane width. Thus, we have only two free parameters in the model κ and $G^{(5)}$.

From the explicit form of the potential in term of the scalars fields

$$V(\phi, \chi) = \frac{\kappa^2}{2Z^2} (Z^2 - \phi^2 - a\chi^2)^2 + \frac{2a^2\kappa^2}{Z^2} \phi^2 \chi^2$$
$$- \frac{4\kappa^2 G^{(5)}}{3Z^2} \phi^2 \left(Z^2 - \frac{1}{3} \phi^2 - a\chi^2 \right)^2, \quad (45)$$

we get the masses for the fields ϕ and χ as being

$$m_\phi = \sqrt{\frac{14}{3}} \kappa, \qquad m_\chi = \sqrt{2a} \kappa, \quad (46)$$

therefore, the parameter κ is explicitly related with the field masses. It offers an opportunity for κ to be the energy scale of the model.

The action for massless Dirac fermion is given by

$$S_f = \int dx^4 dy \sqrt{|g|} [\bar{\Psi} \Gamma^a D_a \Psi - \gamma \eta \bar{\Psi} F(\phi, \chi) \Psi], \quad (47)$$

where γ is a dimensionless parameter and $[\Psi] = M^2$. As the function $F(\phi, \chi) = \phi \chi$ has dimension 3, we have $[\eta] = M^{-2}$.

In order to obtain an expression for the effective coupling constant η in terms of our two free parameters, we check the linear equations of motion (16) and (17) after the change of variables $\alpha_L = e^{-2A} L$ and $\alpha_R = e^{-2A} R$:

$$[\partial_z + \gamma \eta e^A F(\phi, \chi)] L = mR, \quad (48)$$

$$[\partial_z - \gamma \eta e^A F(\phi, \chi)] R = -mL. \quad (49)$$

By performing the following rescaling:

$$z = \lambda \xi, \qquad \partial_z = \lambda^{-1} \partial_\xi, \quad (50)$$

with $[\lambda] = M^{-1}$, the Eqs. (48) and (49) are rewritten as

$$[\partial_\xi + \gamma e^A F(\bar{\phi}, \bar{\chi})] L = \bar{m} R, \quad (51)$$

$$[\partial_\xi - \gamma e^A F(\bar{\phi}, \bar{\chi})] R = -\bar{m} L, \quad (52)$$

where $\bar{\phi} = \phi/Z$, $\bar{\chi} = \chi/Z$ are dimensionless fields. We have set

$$\lambda^{-1} = \eta Z^2, \quad (53)$$

and $\bar{m} = m\lambda$ is a dimensionless constant, this way, the parameter λ^{-1} gives our mass or energy scale.

The choosing of the coupling constant η is a fine-tuning procedure so that the model has the chance of providing a phenomenology in agreement with LHC energy scale. Thus, setting $\eta = \kappa G^{(5)}$, the mass scale results

$$\lambda^{-1} = \kappa, \tag{54}$$

therefore the mass scale is related to the brane width and it is independent of the relation between $G^{(5)}$ and the four-dimensional G constant.

From the kink Eqs. (44), we define the effective brane width as

$$\Delta L = \frac{1}{4a\kappa}. \tag{55}$$

In order for resonances to appear, our model imposes the condition $a \lesssim 0.17$, this gives $\Delta L \gtrsim 1.47\kappa^{-1}$. By considering $\kappa \sim 1$ TeV, we obtain that the brane width is $\gtrsim 10^{-18}$ cm. It is easy to note that if $\kappa > 1$ TeV we get better lower limit for the brane width.

V. CONCLUSIONS

In this work we considered branes constructed with two scalar fields. We considered a simple Yukawa coupling between the two scalars and the spinor field. Depending on the amount of the coupling parameter a between the scalars, the energy momentum density of the branes can be characterized by a two-peak or by a single peak. After [22] we consider this two-peak distribution as characterizing a brane with internal structure. For these more complex branes, the coupling parameter a is small. We investigated the occurrence of massive modes with both chiralities solving numerically the Schrödinger equation and looking for zero modes and possible resonances. For branes with internal structure, we found left- and right-handed resonances together with zero-mode left-handed solutions. The absence of zero-mode solutions for right-handed fermions together with their findings for left-handed ones agrees with the well-known fact that massless fermions must be single-handed in a brane model [32]. With respect to resonances for left-handed fermions, we can resume our conclusions with the following points: (i) Larger values of a correspond to larger peaks of resonance, with corresponding smaller lifetimes. (ii) Above a threshold value of the parameter a, the resonances become too unstable and cease to appear. This coincides with the qualitative change of the energy momentum density of the brane. (iii) Branes with internal structure are more effective in trapping left-fermions. (iv) The lower is the parameter a, the higher is the mass of the resonant mode. This means that branes with internal structure tend to trap matter with larger mass more efficiently in comparison to branes without internal structure. A further investigation on this subject could consider other classes of Yukawa interaction in order to look for possible effects on the massive fermionic resonances.

[1] L. Randall and R. Sundrum, Phys. Rev. Lett. **83**, 3370 (1999).
[2] N. Arkani-Hamed, S. Dimopoulos, and G. Dvali, Phys. Lett. B **429**, 263 (1998).
[3] I. Antoniadis, N. Arkani-Hamed, S. Dimopoulos, and G. Dvali, Phys. Lett. B **436**, 257 (1998).
[4] V. A. Rubakov and M. E. Shaposhnikov, Phys. Lett. B **125**, 139 (1983).
[5] C. Csáki, J. Erlich, C. Grojean, and T. J. Hollowood, Nucl. Phys. **B584**, 359 (2000).
[6] M. Cvetic and H. H. Soleng, Phys. Rep. **282**, 159 (1997).
[7] K. Akama, *Proceedings of The Symposium on Gauge Theory and Gravitation*, edited by K. Kikkawa, N. Nakanishi and H. Nariai (Springer-Verlag, Japan, 1983).
[8] V. A. Rubakov and M. E. Shaposhnikov, Phys. Lett. B **125**, 136 (1983).
[9] M. Visser, Phys. Lett. B **159**, 22 (1985).
[10] P. D. Mannheim (World Scientific, Singapore, 2005).

[11] O. DeWolfe, D. Z. Freedman, S. S. Gubser, and A. Karch, Phys. Rev. D **62**, 046008 (2000).
[12] C. Csáki, J. Erlich, T. J. Hollowood, and Y. Shirman, Nucl. Phys. **B581**, 309 (2000).
[13] M. Gremm, Phys. Lett. B **478**, 434 (2000).
[14] A. Campos, Phys. Rev. Lett. **88**, 141602 (2002).
[15] F. A. Brito, M. Cvetic, and S. C. Yoon, Phys. Rev. D **64**, 064021 (2001).
[16] D. Bazeia, F. A. Brito, and A. R. Gomes, J. High Energy Phys. 11 (2004) 070.
[17] L. Randall and R. Sundrum, Phys. Rev. Lett. **83**, 4690 (1999).
[18] A. Melfo, N. Pantoja, and A. Skirzewski, Phys. Rev. D **67**, 105003 (2003).
[19] D. Bazeia, A. R. Gomes, and L. Losano, Int. J. Mod. Phys. A **24**, 1135 (2009); arXiv:0708.3530.
[20] N. Barbosa-Cendejas and A. Herrera-Aguilar, Phys. Rev. D **73**, 084022 (2006).

[21] N. Barbosa-Cendejas, A. Herrera-Aguilar, M. A. Reyes, and C. Schubert, Phys. Rev. D **77**, 126013 (2008).

[22] D. Bazeia, C. Furtado, and A. R. Gomes, J. Cosmol. Astropart. Phys. 02 (2004) 002.

[23] D. Bazeia and A. R. Gomes, J. High Energy Phys. 05 (2004) 012.

[24] D. Bazeia, J. R. Nascimento, R. F. Ribeiro, and D. Toledo, J. Phys. A **30**, 8157 (1997).

[25] D. Bazeia, F. A. Brito, and H. Boschi-Filho, J. High Energy Phys. 04 (1999) 028.

[26] D. Bazeia, M. J. dos Santos, and R. F. Ribeiro, Phys. Lett. A **208**, 84 (1995).

[27] E. Witten, Nucl. Phys. **B249**, 557 (1985).

[28] M. Hatsuda and M. Sakaguchi, Nucl. Phys. **B577**, 183 (2000).

[29] S. Randjbar-Daemi and M. Shaposhnikov, Phys. Lett. B **492**, 361 (2000).

[30] S. Mouslopoulos, J. High Energy Phys. 05 (2001) 038.

[31] S. L. Dubovsky, V. A. Rubakov, and P. G. Tinyakov, Phys. Rev. D **62**, 105011 (2000).

[32] C. Ringeval, P. Peter, and J.-P. Uzan, Phys. Rev. D **65**, 044016 (2002).

[33] W. Bietenholz, A. Gfeller, and U.-J. Wiese, J. High Energy Phys. 10 (2003) 018.

[34] R. Koley and S. Kar, Classical Quantum Gravity **22**, 753 (2005).

[35] A. Melfo, N. Pantoja, and J. D. Tempo, Phys. Rev. D **73**, 044033 (2006).

[36] G. Gibbons, K. Maeda, and Y. Takamizu, Phys. Lett. B **647**, 1 (2007).

[37] Yu-Xiao Liu, Li-Da Zhang, Li-Jie Zhang, and Yi-Shi Duan, Phys. Rev. D **78**, 065025 (2008).

[38] Y.-X. Liu, X.-H. Zhang, L.-D. Zhang, and Y.-S. Duan, J. High Energy Phys. 02 (2008) 067.

[39] Y.-X. Liu, L.-D. Zhang, S.-W. Wei, and Y.-S. Duan, J. High Energy Phys. 08 (2008) 041.

[40] R. Davies and D. P. George, Phys. Rev. D **76**, 104010 (2007).

[41] R. Jackiw and C. Rebbi, Phys. Rev. D **13**, 3398 (1976).

[42] F. Cooper, A. Khare, and U. Sukhatme, Phys. Rep. **251**, 267 (1995).

[43] A. de Felice and C. Ringeval, Phys. Lett. B **671**, 158 (2009).

[44] R. Gregory, V. A. Rubakov, and S. M. Sibiryakov, Phys. Rev. Lett. **84**, 5928 (2000).

[45] P. M. Llatas, Phys. Lett. B **514**, 139 (2001).

[46] Y. Liu, J. Yang, Z. Zhao, C. Fu, and Y. Duan, arXiv:0904.1785.

[47] Y. Grossman and M. Neubert, Phys. Lett. B **474**, 361 (2000).